### **CONFERENCE PRE-PRINT**

# SCALING OF THE H-MODE ELECTRON SEPARATRIX DENSITY BASED ON ENGINEERING PARAMETERS FROM C-MOD, AUG AND JET DATA

D. SILVAGNI¹, O. GROVER¹, A. STAGNI², J. W. HUGHES³, M. A. MILLER³, B. LOMANOWSKI⁴, G. CIRAOLO⁵, W. DEKEYSER⁶, M. DUNNE¹, T. EICH², L. FRASSINETTI⁶, C. GIROUD⁶, T. HAPPEL¹, I. JEPU⁶, A. KALLENBACH¹, A. KIRJASUO¹⁰, A. KUANG⁷, F. LATINI¹¹, T. LUDA¹, D. MOULTON⁶, O. PAN¹, C. PEREZ VON THUN¹², T. PÜTTERICH¹, S. A. SILBURN⁶, H. J. SUN⁶, H. ZOHM¹, THE ASDEX UPGRADE TEAM⁶, JET CONTRIBUTORS⁶ AND THE EUROFUSION TOKAMAK EXPLOITATION TEAM⁶

#### **Abstract**

The electron density at the separatrix  $(n_{e, \rm sep})$  plays a central role in balancing energy confinement, detachment achievement, and ELM suppression in tokamaks, thereby influencing core-edge integration. To study what determines this key parameter, a database of H-mode separatrix density measurements from Alcator C-Mod, ASDEX Upgrade, and JET tokamaks has been assembled using a consistent analysis method across all devices. This dataset is used to derive a regression scaling law based solely on engineering parameters, and the results are compared to predictions from the two-point model. The agreement found is notable: both the regression and model provide similar parameter dependencies and tokamak-specific multiplicative constants. Building on this agreement, a fully predictive formula that combines the regression dependencies and the two-point model multiplicative constant is proposed. This formula is able to estimate  $n_{e, \rm sep}$  across the three machines within a factor of 1.5.

#### 1. INTRODUCTION

One of the key open challenges on the pathway to building a fusion power plant based on the tokamak concept is the determination of a so-called core-edge integrated plasma scenario. In such a scenario, the plasma needs to combine high fusion energy production with acceptable heat and particle loads on first-wall materials, the latter usually achieved via pronounced detachment [1]. Moreover, transient heat loads induced by edge-localized modes (ELMs) should be avoided [2], along with plasma disruptions. The electron density at the separatrix  $n_{e,\text{sep}}$  is a key parameter that influences the above-mentioned processes: It affects H-mode confinement by altering the pedestal stability [3, 4, 5, 6, 7], detachment achievement by influencing the required impurity concentration needed to detach [8, 9, 10], access to no-ELM regimes [11, 12, 13, 14], and it poses an upper limit to H-mode operation (the so-called density limit) [15, 16, 17]. Therefore, reliable, quantitative predictions of  $n_{e,\text{sep}}$  are essential for evaluating and designing next-step fusion experiments and reactors.

Several previous studies highlighted the connection between the (upstream) separatrix density and the (downstream) divertor target conditions, via the so-called two-point model [18, 19]. At DIII-D [20] and JET [21],  $n_{e,\text{sep}}$  has been shown to be clearly linked to the measured electron temperature in the divertor region, as expected from the two-point model equations. In ASDEX Upgrade (AUG), a strong connection between the electron separatrix density and the sub-divertor neutral pressure  $p_{0,\text{div}}$  has been observed both experimentally [22] and in simulations [23]. This finding has been reconciled with the two-point model by relating the target ion flux to the divertor neutral pressure. More recently, similar relationships connecting  $n_{e,\text{sep}}$  to the divertor neutral pressure have been observed also in TCV [24], JET and Alcator C-Mod (C-Mod) [25].

It is important to note that  $p_{0,\rm div}$  can be regarded as an engineering parameter, since it is primarily set by the applied gas puff level and effective pumping speed of the system [22], allowing for  $n_{e,\rm sep}$  predictions based only on engineering parameters. Indeed, in AUG this approach enabled core-pedestal-SOL integrated modeling of plasma discharges using solely engineering parameters as input [26]. However, the  $n_{e,\rm sep}$  formulas used so far always depend on tokamak-specific constants, which make extrapolation efforts challenging. Also, single-machine studies cannot unveil the size dependence of  $n_{e,\rm sep}$ , an important topic for extrapolation.

<sup>&</sup>lt;sup>1</sup>Max Planck Institute for Plasma Physics, Garching, Germany

<sup>&</sup>lt;sup>2</sup>Consorzio RFX, Padova, Italy

<sup>&</sup>lt;sup>3</sup>MIT Plasma Science and Fusion Center, Cambridge, MA, United States of America

<sup>&</sup>lt;sup>4</sup>Oak Ridge National Laboratory, Oak Ridge, TN, United States of America

<sup>&</sup>lt;sup>5</sup>IRFM, CEA, St. Paul-Lez-Durance, France

 $<sup>^6</sup> KU$  Leuven, Department of Mechanical Engineering, Leuven, Belgium

<sup>&</sup>lt;sup>7</sup>Commonwealth Fusion Systems, Devens, MA, United States of America

<sup>&</sup>lt;sup>8</sup>KTH Royal Institute of Technology, Division of Electromagnetic Engineering and Fusion Science, Stockholm, Sweden

<sup>&</sup>lt;sup>9</sup>UKAEA, Culham Science Centre, Abingdon, United Kingdom of Great Britain and Northern Ireland

<sup>&</sup>lt;sup>10</sup>VTT, Espoo, Finland

<sup>&</sup>lt;sup>11</sup> Tuscia University, Department of Economics, Engineering, Society and Business (DEIM), Viterbo, Italy

<sup>&</sup>lt;sup>12</sup>Institute of Plasma Physics and Laser Microfusion, Warsaw, Poland

<sup>&</sup>lt;sup>a</sup>See author list of H. Zohm, 2024 Nucl. Fusion 64 112001

<sup>&</sup>lt;sup>b</sup>See author list of C. F. Maggi, 2024 Nucl. Fusion 64 112012

<sup>&</sup>lt;sup>c</sup>See author list of E. Joffrin, 2024 Nucl. Fusion 64 112019

To fill this gap, a multi-machine database of H-mode  $n_{e,\mathrm{sep}}$  values evaluated with the same procedure has been assembled, using data from three metal-wall devices: Alcator C-Mod, ASDEX Upgrade and JET. The collected data have been used to derive a cross-machine scaling law of  $n_{e,\mathrm{sep}}$ , with machine specific multiplication constants. Regression analysis revealed that  $n_{e,\mathrm{sep}}$  reduces with increasing plasma minor radius (i.e. machine size), consistent with the associated increase of SOL connection length. The dependence of  $n_{e,\mathrm{sep}}$  to other engineering parameters, such as  $p_{0,\mathrm{div}}$ ,  $I_p$ ,  $B_t$ ,  $P_{\mathrm{SOL}}/R$ , is also discussed and compared to the  $n_{e,\mathrm{sep}}$  expression given by the two-point model. Overall, the agreement found is notable, despite slight discrepancies in the exponents of  $p_{0,\mathrm{div}}$  and  $B_t$  which are further discussed. Perhaps more importantly, the two-point model multiplicative constant in the  $n_{e,\mathrm{sep}}$  expression is compared to the regression-inferred tokamak-specific constants, finding good agreement. This allowed the introduction of a predictive  $n_{e,\mathrm{sep}}$  formula based on two-point model multiplicative constant and regression-based dependencies which proved able to predict  $n_{e,\mathrm{sep}}$  within a factor 1.5 across the three devices.

The content is organized as follows. In section 2 the database is described and co-correlations between parameters are discussed. In section 3, the cross-machine  $n_{e,\rm sep}$  scaling law is introduced. In section 4, the two-point model expression for  $n_{e,\rm sep}$  is derived and compared to the regression findings. The predictive formula and its applicability are discussed in section 5, while the conclusions are outlined in section 6.

#### 2. DATABASE

The database used in this work builds on the one assembled in [25], with some additional features that are discussed at the end of this section. The key characteristics of this database are:

- 1. Use of similar closed divertor (lower single null) configurations across the three devices;
- 2. H-mode plasmas in favorable configuration—in JET with ELMs, in C-Mod without ELMs (the so-called EDA H-mode [27]), while in AUG a mixture of ELMy and no-ELM plasmas;
- 3. Unseeded plasmas in JET and C-Mod, while both unseeded and seeded plasmas in AUG;
- 4. Stationary phases in both plasma and sub-divertor neutral pressure, the latter measured by baratrons along vertical pipes, see Fig. 1 in Ref. [25];
- 5. Separatrix parameters evaluated with exactly the same procedure based on power balance in each device.

Concerning the last point, edge electron temperature and density profiles measured by Thomson scattering have been mapped to the outer midplane and fit with the same function in each device. Then, scrape-off layer (SOL) power balance has been applied to determine the electron temperature at the separatrix  $T_{e,\rm sep}$ , ensuring that the same pre-factors are used when evaluating  $T_{e,\rm sep}$ . A notable aspect of this power balance analysis is the direct evaluation of the inter-ELM temporal derivative of the plasma stored energy, dW/dt, via fast magnetic equilibrium reconstruction—a term that is often neglected or approximated as a constant fraction of the absorbed heating power. For additional details on the separatrix evaluation procedure, the reader is referred to [25].

	C-Mod	AUG	JET
Discharges	111	43	45
$I_{\rm p}$ (MA)	0.6-1.4	0.6-1.2	1.8-2.6
$B_{\rm t}$ (T)	4.5–7.8	1.8-2.6	2.1-3.3
$q_{95}$	2.9-7.2	3.1-6.9	2.9-4.0
$P_{\mathrm{SOL}}\left(\mathrm{MW}\right)$	0.3-2.5	0.7-12.8	4.9–18.8
$\overline{n}_e \ (10^{19} \ {\rm m}^{-3})$	16.9-53.6	4.8-13.2	3.9-8.5
$p_{0,\mathrm{div}}$ (Pa)	0.7-16.9	0.2-7.2	0.03-0.9
$R_{\rm geo}$ (m)	0.67-0.68	1.61-1.65	2.89-2.94
$a_{ m geo}$ (m)	0.21-0.22	0.49-0.53	0.89-0.95

TABLE 1. Parameter range of the assembled database.

The main plasma parameters of the assembled database are summarized in Table 1. Compared to the database shown in [25], additional high-field plasma at  $B_t \approx 7.8 \,\mathrm{T}$  from C-Mod have been included [28]. Further, the JET dataset has been restricted

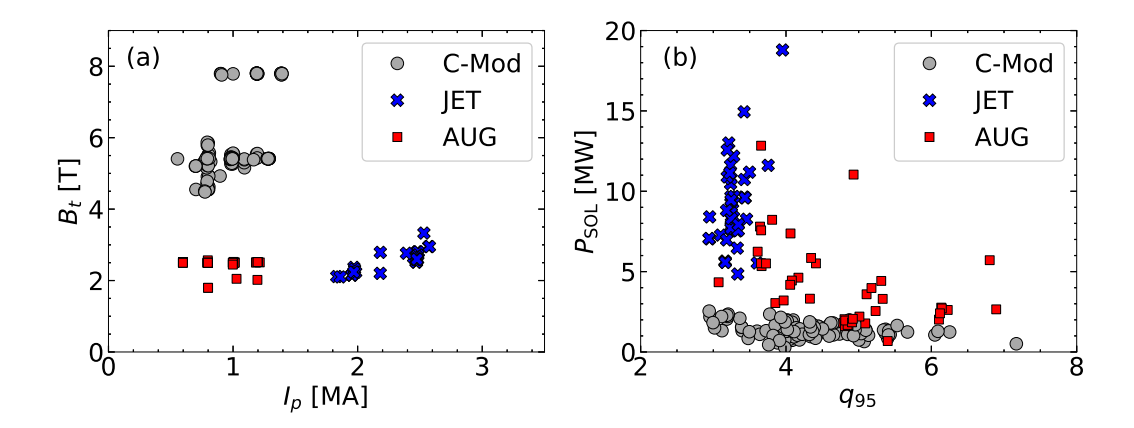


FIG. 1. On-axis toroidal magnetic field vs. plasma current (a) and power crossing the separatrix vs. edge safety factor (b) for the analyzed C-Mod (circles), AUG (squares) and JET (crosses) datasets.

to low triangularity plasmas only ( $\delta_{\rm av} < 0.26$ ). The reason for this choice resides in the additional dependency of  $n_{e,{\rm sep}}$  on triangularity found in JET 'vertical-vertical' (V-V) target configuration [25], which is the divertor configuration used in this study for JET. This dependency deserves a detailed study that goes beyond the scope of this paper, therefore it is left as a topic for future research.

Figure 1 shows the achieved variation in plasma current  $(I_p)$ , on-axis toroidal magnetic field  $(B_t)$ , safety factor evaluated at the 95% magnetic flux surface  $(q_{95})$  and power entering the SOL  $(P_{SOL})$  in the three devices. A satisfactory variation and de-correlation of  $I_p$  and  $B_t$  is obtained in AUG and C-Mod, which is reflected in the broad range of  $q_{95}$  values spanned in both devices. In JET, while a good variation in  $I_p$  and  $B_t$  is obtained, these two values are mainly correlated, resulting in a small variation of  $q_{95}$ . Historically, this is due to the fact that experiments in V-V configuration at JET were mainly executed to be self-similar to ITER [29, 30], which is expected to operate a low  $q_{95}$ . The power entering

the SOL exhibits also a good variation, as well as the line-averaged density  $(\overline{n}_e)$  which is spanning more than one order of magnitude across the three devices, see table 1. The divertor neutral pressure  $p_{0,\mathrm{div}}$ , measured by a baratron located in the sub-divertor region [25], varies by about two orders of magnitude.

The tokamaks analyzed in this study have a nearly constant aspect ratio  $A=R_{\rm geo}/a_{\rm geo}=3.0-3.3$ , where  $R_{\rm geo}$  and  $a_{\rm geo}$  are the geometrical major and minor radii, respectively. As a result,  $R_{\rm geo}$  and  $a_{\rm geo}$  are fully correlated, and cannot be used together as independent variables in the regression analysis. Therefore, we use only  $a_{\rm geo}$  as a regression variable in this study, while  $R_{\rm geo}$  is employed solely as a normalization factor for  $P_{\rm SOL}$ . This choice is motivated by theoretical considerations, which will be discussed further in section 4.

Figure 2 shows the correlation matrix of the variables chosen for regression analysis. A good level of de-correlation is achieved between  $I_p$ ,  $B_t$ ,  $P_{\rm SOL}$  and  $p_{0,\rm div}$ . The same cannot be said for  $a_{\rm geo}$ , which shows a positive correlation with  $I_p$  and a negative correlation with  $B_t$ . Therefore, particular care should be taken with the  $a_{\rm geo}$  dependencies found in this study.

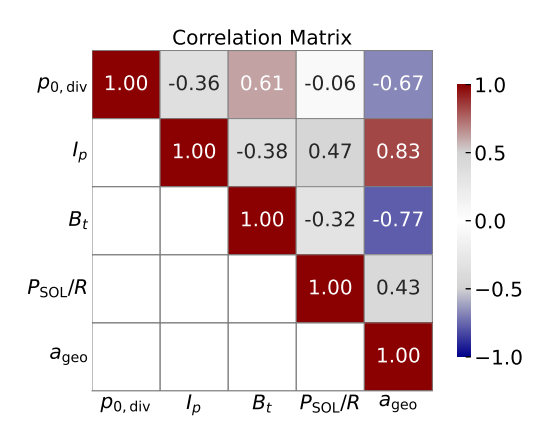


FIG. 2. Correlation matrix of the variables used for the regression analysis.

#### 3. MULTI-MACHINE SCALING LAW OF THE SEPARATRIX ELECTRON DENSITY

To model the variable  $n_{e, \text{sep}}$ , the following power law is considered  $n_{e, \text{sep}} = C_{\text{dev}} \cdot p_{0, \text{div}}^{\alpha_p} \cdot I_p^{\alpha_I} \cdot B_t^{\alpha_B} \cdot \left(\frac{P_{\text{SOL}}}{R_{\text{geo}}}\right)^{\alpha_P/R} \cdot a_{\text{geo}}^{\alpha_a}$ , where  $C_{\text{dev}}$  is a device-specific multiplication constant and  $\alpha_X$  is the exponent of the independent variable X. This expression has been chosen to facilitate comparisons with the two-point model, as will be discussed in the next section. Applying a generalized linear model with Gaussian likelihood and the logarithmic link function, the following scaling law is obtained:

$$n_{e,\text{sep,sc}}[10^{19}\,\text{m}^{-3}] = C_{\text{dev}} \cdot (p_{0,\text{div}}[\text{Pa}])^{0.20 \pm 0.03} \cdot (I_p[\text{MA}])^{0.03 \pm 0.09} \cdot (B_t[\text{T}])^{-0.26 \pm 0.11} \cdot \left(\frac{P_{\text{SOL}}}{R_{\text{geo}}} \left[\frac{\text{MW}}{\text{m}}\right]\right)^{0.19 \pm 0.04} \cdot (a_{\text{geo}}[\text{m}])^{-0.47 \pm 1.92},$$
(1)

with  $C_{\rm dev}$  being  $6.3 \pm 2.4$  for C-Mod,  $2.0 \pm 0.9$  for AUG, and  $3.0 \pm 2.8$  for JET. The normalized root mean square error is NRMSE = 19 \%, while  $R^2 = 0.91$ . Figure 3 shows the comparison between the experimental  $n_{e, \text{sep}}$  data and those predicted by the scaling law. A satisfactory agreement is found across more than one order of magnitude. Regression analysis reveals that the two parameters driving an increase in  $n_{e,\text{sep}}$  are the divertor neutral pressure and  $P_{\text{SOL}}/R_{\text{geo}}$ , both exhibiting similar exponents ( $\sim 0.2$ ). The dependence on  $p_{0,\mathrm{div}}$  is consistent with results from single-machine analyses [22, 25], with an exponent that most closely resembles the value reported for C-Mod, see Fig. 4(a). A comparable relationship  $(n_{e, {\rm sep}} \propto p_{0, {\rm div}}^{0.22})$  has also been found in recent SOLPS-ITER gas scan simulations of the ITER Q=10 baseline scenario [31], increasing confidence in the applicability of this scaling in plasmas with high neutral opacity. The observed dependence of  $n_{e,sep}$  on  $P_{SOL}$  aligns with previous studies at JET [21, 32] and DIII-D [20], which also reported a mild positive correlation between the two quantities.

The two parameters that lead to a decrease in  $n_{e,\text{sep}}$  when increased are the plasma minor radius and the toroidal magnetic field  $B_t$ . A negative dependence on  $B_t$  was also ob-

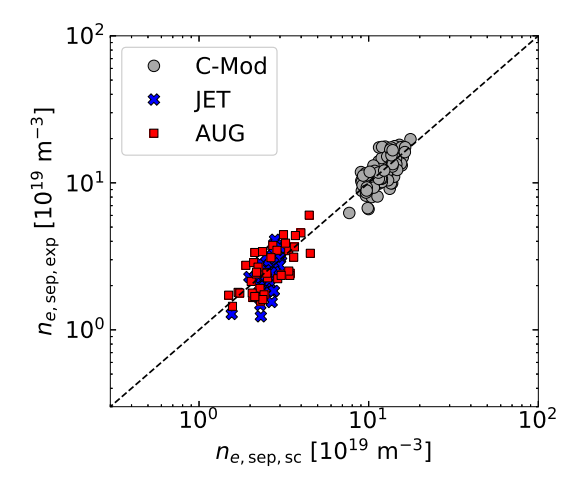


FIG. 3. Experimental  $n_{e,\rm sep}$  values against those predicted by Eq. 1 for C-Mod (gray circles), AUG (red squares) and JET (blue triangles).

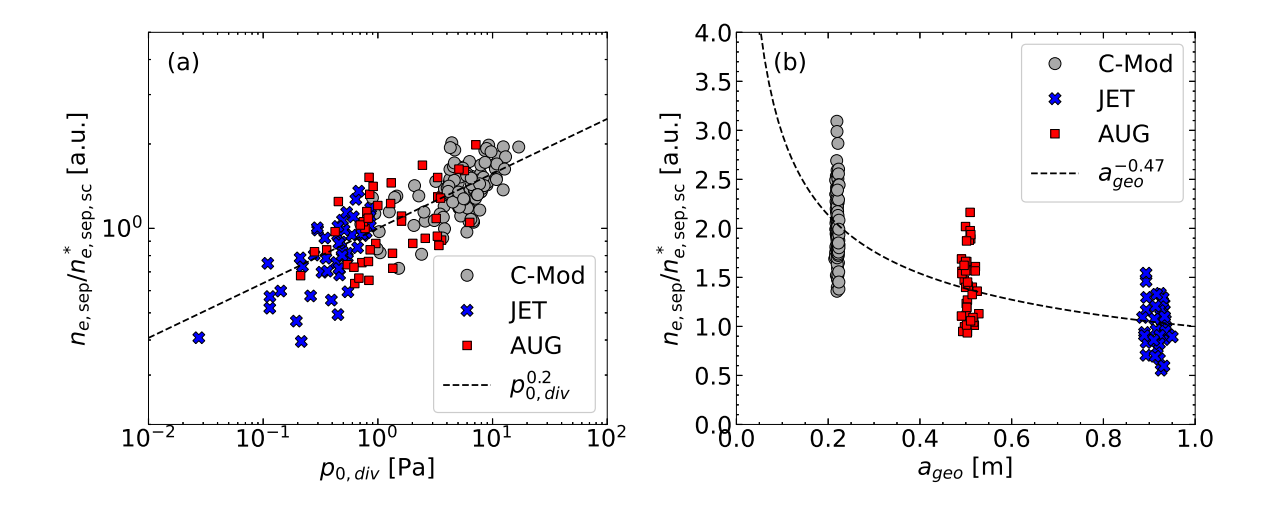


FIG. 4. Experimental  $n_{e,\text{sep}}$  values normalized by the scaling law in Eq. 1, excluding the dependence on the parameter shown on the x-axis:  $p_{0,\text{div}}$  in (a) and  $a_{\text{geo}}$  in (b). The residual scaling dependence on  $p_{0,\text{div}}$  and  $a_{\text{geo}}$  is plotted as a dashed line.

served experimentally in DIII-D [20], and was correlated with an increase of the SOL radiative fraction as  $B_t$  increases. Additionally, several tokamaks have reported a reduction in  $n_{e,ped}$  with increasing  $B_t$  at fixed plasma current [28, 20, 33], a trend that would be consistent with a corresponding decrease in  $n_{e,\mathrm{sep}}$ .

The other quantity exhibiting a relatively strong negative correlation with  $n_{e,\text{sep}}$  is  $a_{\text{geo}}$ , as also shown in Fig. 4(b). This finding will be compared to the two-point model expectations in the next section. However, as expected from the discussion in section 2, a large error is associated to the  $a_{\rm geo}$  exponent, which calls for particular caution in the interpretation of this dependency.

Lastly, the multi-machine regression finds no relevant dependence of  $n_{e,\text{sep}}$  on the plasma current  $I_p$ . This result is consistent with previous observations in each single device [22, 25], which also reported an absent correlation with  $I_p$  upon normalizing  $n_{e,\text{sep}}$  to the  $p_{0,\text{div}}$  dependency. It should be noted that when  $n_{e,\text{sep}}$  is not normalized to the  $p_{0,\text{div}}$  dependency, a mild correlation with the plasma current is typically observed [22, 20, 34]. However, this mild correlation is thought to be due to the larger gas puff usually required at higher current to avoid impurity accumulation in H-mode. Indeed, employing a Z-test to our variables reveals that  $p_{0,\text{div}}$  is a very strong statistical predictor (p-value of zero), while  $I_p$  is not a statistically significant predictor (p-value of 0.735).

## 4. TWO-POINT MODEL EXPRESSION FOR $n_{e, \mathrm{sep}}$ AS A FUNCTION OF ENGINEERING PARAMETERS

In this section, an expression for  $n_{e,\text{sep}}$  as a function of engineering parameters will be derived. This treatment is an extension of the one introduced by Kallenbach et al. in Ref. [22]. A SOL flux tube connecting the outer midplane to the outer divertor target is considered, as typically done with two-point modeling [18]. Key assumptions of the model used here are: (1) Ions and electrons have the same temperature,  $T_i = T_e = T$ , with temperatures expressed in eV; (2) The upstream parallel velocity is zero, while the velocity at the target is the ion sound speed for an isothermal flow  $c_s = \sqrt{\frac{2eT}{m_i}}$ , where e is the electron charge and  $m_i$  the ion mass; (3) All the power enters the flux tube at the upstream position and is transported in the parallel direction solely by electron conduction. Momentum and power sinks along the flux tube are parametrized by loss factors, defined as  $(1-f_{\mathrm{mom}})p_{\mathrm{tot,u}}=p_{\mathrm{tot,d}}$  and  $(1-f_{\mathrm{pow}})P_{\mathrm{u}}=P_{\mathrm{d}}$  for the momentum and power, respectively. The subscripts 'u' and 'd' stand for 'upstream' and 'downstream' positions along the flux tube, while P indicates the power and  $p_{\mathrm{tot}}$  the total plasma pressure, given by the sum of static and dynamic pressures.

The four basic equations of the two-point model are given by momentum and power conservation, Fourier's law to describe heat transport in the parallel direction, and a target boundary condition, which defines the target heat flux at the sheath entrance. These equations read:

$$(1 - f_{\text{mom}})n_{\text{u}}T_{\text{u}} = 2n_{\text{d}}T_{\text{d}} \tag{2}$$

$$(1 - f_{\text{pow}})q_{||,u}A_{\perp,\text{SOL},u} = q_{||,d}A_{\perp,\text{SOL},d} \quad \Rightarrow \quad (1 - f_{\text{pow}})q_{||,u} = q_{||,d}b\frac{B_{\text{u}}}{D}$$
 (3)

$$(1 - f_{pow})q_{||,u}A_{\perp,SOL,u} = q_{||,d}A_{\perp,SOL,d} \Rightarrow (1 - f_{pow})q_{||,u} = q_{||,d}b\frac{B_{u}}{B_{d}}$$

$$T_{u} = \left(\frac{7q_{||,u}L_{||}}{2\kappa_{0}}\right)^{2/7}$$

$$q_{||,d} = \gamma eT_{d}\Gamma_{||,d} \Rightarrow q_{||,d} = \gamma eT_{d}n_{d}c_{s,d}$$

$$(5)$$

$$q_{\parallel,d} = \gamma e T_{\rm d} \Gamma_{\parallel,d} \quad \Rightarrow \quad q_{\parallel,d} = \gamma e T_{\rm d} n_{\rm d} c_{\rm s,d}$$
 (5)

where  $q_{||}$  indicates the heat flux parallel to the magnetic field,  $A_{\perp,\mathrm{SOL}}$  the SOL flux bundle area perpendicular to the magnetic field line, B the total magnetic field,  $L_{||}$  the SOL parallel connection length between the outer midplane and the target,  $\kappa_0$  is the parallel electron conductivity coefficient,  $\gamma$  is the total sheath heat transmission factor,  $\Gamma_{||,d} = n_{\rm d}c_{s,\rm d}$  is the parallel ion flux density (particles/m²/s) at the sheath entrance, and  $b = \lambda_{\rm int}/\lambda_q = 1 + 1.64S/\lambda_q$  is the divertor broadening factor, with  $\lambda_q$  and  $\lambda_{\rm int}$  being the outer midplane heat flux decay length and the integral heat flux decay length at the target, respectively, while S is the broadening parameter. For a detailed overview of  $\lambda_q$ ,  $\lambda_{\rm int}$  and S, the reader is referred to Ref. [35, 36, 37]. Compared to the equations typically used for the two-point model [18, 22, 21], the main difference is in the factor  $B_{\rm u}/B_{\rm d}$  in Eq. 3, which is typically approximated to be  $B_{t,\rm u}/B_{t,\rm d}\sim R_{\rm d}/R_{\rm u}$ . However, to potentially model also alternative divertor configurations [38, 39] which could have different  $B_{\rm p,u}/B_{\rm p,d}$  ratios, this approximation is not made here. Also, it is worth noting that the broadening factor b accounts for power losses perpendicular to the magnetic flux bundle in the divertor region. Therefore, in this formulation, the power loss factor  $f_{\rm pow}$  primarily reflects losses due to radiation and charge exchange reactions. A full derivation of Eq. 3 is described in the Appendix.

Combining Eq. 2, 3, 4 and 5, an expression for the upstream electron density  $n_{e,u}$  as a function of  $q_{||,u}$ ,  $L_{||}$  and  $\Gamma_{||,d}$  is obtained:

$$n_{e,u} = \frac{2(1 - f_{\text{pow}})^{1/2}}{(1 - f_{\text{mom}})} \left(\frac{2\kappa_0}{7}\right)^{2/7} \frac{1}{e} \left(\frac{B_d}{B_u} \frac{1}{\gamma 2b}\right)^{1/2} m_i^{1/2} q_{||,u}^{3/14} L_{||}^{-2/7} \Gamma_{||,d}^{1/2}, \tag{6}$$

which differs from the one derived in [22] only by the additional  $\sqrt{B_{\rm d}/B_{\rm u}}$  factor. This expression highlights the primary physics parameters affecting  $n_{e,{\rm sep}}$ . Both the ion flux density at the target and the upstream heat flux drive an increase in  $n_{e,{\rm sep}}$ , while extending the connection length between the outer midplane and the target reduces  $n_{e,{\rm sep}}$ . While Eq. 6 is extremely insightful to study what drives changes in  $n_{e,{\rm sep}}$ , it is of reduced usage for what concerns extrapolations, as the ion flux density at the target can be estimated only with the help of modeling. Therefore, in the next paragraphs a series of assumptions will be introduced to express  $n_{e,{\rm sep}}$  as a function of engineering parameters.

To express  $q_{||,u}$  and  $L_{||}$  as a function of  $I_p$  and  $B_t$ , the poloidally-averaged poloidal magnetic field  $\langle B_p \rangle = \mu_0 I_p/(2\pi a_{\rm geo}\hat{\kappa})$  and the cylindrical safety factor  $q_{\rm cyl} = \hat{\kappa} a_{\rm geo} B_t/(R_{\rm geo} \langle B_p \rangle)$  are introduced, with  $\hat{\kappa} = \sqrt{(1 + \kappa^2 (1 + 2\delta^2 - 1.2\delta^3))/2}$  being an effective plasma elongation corrected for the triangularity, a parameter introduced in Ref. [40] to account for the real geometrical plasma shape while using a cylindrical approximation. In this way,  $L_{||}$  can be expressed as:

$$L_{||} = l^* \pi R_{\text{geo}} q_{\text{cyl}} = l^* \frac{2}{\mu_0} (\pi a_{\text{geo}} \hat{\kappa})^2 \frac{B_t}{I_p}, \tag{7}$$

where  $l^*$  is a constant describing the deviation of the real connection length from the approximated formula  $\pi R_{\rm geo} q_{\rm cyl}$ . For the divertor configurations analyzed in this study,  $l^*$  is about 1.2, 1.3, and 1.1 for C-Mod, AUG and JET, respectively. To calculate this number the SOL connection length has been evaluated from the magnetic field line at approximately half  $\lambda_q$  [25]. Clearly,  $l^*$  can be larger when alternative divertor configurations are considered.

The upstream parallel heat flux can be rewritten as:

$$q_{||,\mathbf{u}} = \frac{f_{\text{out}} P_{\text{SOL}}}{A_{\perp,\text{SOL},\mathbf{u}}} = \frac{f_{\text{out}} P_{\text{SOL}} B_{\mathbf{u}}}{2\pi R_{\mathbf{u}} \lambda_q B_{p,\mathbf{u}}} = \frac{f_{\text{out}} P_{\text{SOL}} B_t}{C_{\text{geo}} 2\pi R_{\text{geo}} \lambda_q \langle B_p \rangle} = \frac{f_{\text{out}} \hat{\kappa} P_{\text{SOL}} a_{\text{geo}} B_t}{C_{\text{geo}} \lambda_q \mu_0 R_{\text{geo}} I_p}, \tag{8}$$

where  $f_{\rm out}$  is the fraction of  $P_{\rm SOL}$  going towards the outer target, and  $C_{\rm geo}$  is a geometrical constant defined as  $R_{\rm u}B_{p,\rm u}/B_{\rm u}=C_{\rm geo}R_{\rm geo}\langle B_p\rangle/B_t$ , which is approximately 2.35 for the three tokamaks.

Following the same argument introduced in [22], it is assumed that the neutral flux density,  $\Gamma_0$ , measured in the sub-divertor region equals the ion flux density perpendicular to the target,  $\Gamma_{\perp,d}$ . Assuming a Maxwellian distribution function of the neutrals at room temperature, the neutral flux density can be converted to a neutral pressure via the formula  $\Gamma_0 = \frac{1}{4} n_0 \sqrt{\frac{8eT_0}{\pi m_0}} = (2\pi m_0 e T_0)^{-1/2} p_0 = C_0 p_0$ , where  $C_0 = 1.1 \times 10^{23}$  atoms/m²/s/Pa. Therefore, the parallel ion flux density can be rewritten

$$\Gamma_{\parallel,d} = \frac{\Gamma_{\perp,d}}{\sin(\alpha_{\text{div}})} \approx \frac{\Gamma_0}{\sin(\alpha_{\text{div}})} = \frac{C_0 p_0}{\sin(\alpha_{\text{div}})},$$
(9)

where  $\alpha_{\rm div}$  is the magnetic field line grazing angle at the outer target. Inserting Eq. 7, 8 and 9 into Eq. 6, the following expression for  $n_{e,\rm sep}$  as a function of engineering parameters is obtained:

$$n_{e,\text{sep}} = C_{\text{2pt}} \left(\frac{P_{\text{SOL}}}{R_{\sigma eo}}\right)^{3/14} I_p^{1/14} B_t^{-1/14} a_{\text{geo}}^{-5/14} p_{0,\text{div}}^{1/2},$$
(10)

with  $C_{2pt}$  being:

$$C_{\text{2pt}} = \frac{2(1 - f_{\text{pow}})^{1/2}}{(1 - f_{\text{mom}})} \left(\frac{\kappa_0}{7l^*}\right)^{2/7} \frac{\mu_0^{1/14} \pi^{-4/7}}{e} \left(\frac{f_{\text{out}}}{C_{\text{geo}} \lambda_q}\right)^{3/14} \left(\frac{B_{\text{d}}}{B_{\text{u}}} \frac{C_0 m_i}{2\gamma b \cdot \sin(\alpha_{\text{div}})}\right)^{1/2} \hat{\kappa}^{-5/14} 10^{12/7}.$$
(11)

In these equations, all quantities are expressed in SI units, except for  $I_p$  (MA),  $P_{\rm SOL}/R_{\rm geo}$  (MW/m) and  $\kappa_0=2275\,{\rm W\,m^{-1}}$  eV $^{-7/2}$ 

The exponents obtained for  $P_{\rm SOL}/R_{\rm geo}$ ,  $I_p$  and  $a_{\rm geo}$  are similar to those found with regression analysis, which is remarkable given the simplicity of the two-point model. However, the exponents of  $p_{0,\rm div}$  and  $B_t$  are somewhat stronger and weaker in magnitude, respectively, than those found in the regression. This discrepancy could stem from additional hidden dependencies of the loss factors on these parameters. Indeed, in DIII-D it was found that the SOL radiative fraction increases as  $B_t$  rises at constant current [20]. This behavior, which could be due to the additional SOL volume available due to the increased connection length, would decrease  $(1-f_{\rm pow})$  when  $B_t$  rises, potentially explaining the stronger  $B_t$  negative exponent found in the regression.

Similarly, SOL power losses are known to increase with decreasing plasma temperature in the divertor region  $T_{\rm d}$  [18, 21] or, equivalently, to increase as the neutral pressure rises [41]. This would cause  $(1-f_{\rm pow})$  to decrease when  $p_{0,{\rm div}}$  rises, which, in turn, could explain the lower positive exponent of  $p_{0,{\rm div}}$  found in the regression.

Of particular interest for prediction capabilities is the comparison of the multiplicative constant obtained from the two-point model,  $C_{\rm 2pt}$ , with the device-specific multiplicative constant inferred through regression,  $C_{\rm dev}$ . In Table 2, the main parameters used to evaluate  $C_{\rm 2pt}$  in the three machines are summarized. The quantities directly evaluated from the equilibrium are  $l^*$ ,  $\alpha_{\rm div}$ ,

	C-Mod	AUG	JET
$f_{\text{out}}$	0.50	0.65	0.65
$l^*$	1.17	1.31	1.09
$\alpha_{ m div}$ (degree)	0.65	3.30	2.50
$S/\lambda_q$	1.00	0.75	0.50
$B_{ m d}/B_{ m u}$	1.42	1.32	1.29
$C_{ m geo}$	2.34	2.51	2.29
$\hat{\kappa}$	1.48	1.40	1.43
$C_{2\mathrm{pt}}$	6.26	2.2	2.85

TABLE 2. Summary of parameter values used to evaluate  $C_{2\text{pt}}$  in the three tokamaks.

 $B_{
m d}/B_{
m u}$ ,  $C_{
m geo}$  and  $\hat{\kappa}$ . In this study, the upstream position is defined as the outer midplane. The fraction of power flowing to the outer target,  $f_{
m out}$ , has been chosen to be 0.5 in C-Mod [42, 43], and 0.65 in AUG and JET [44], following experimental measurements. The values for  $S/\lambda_q$ , which in turn set the broadening factor  $b=1+1.64S/\lambda_q$ , are based on the experimental values found in the ITPA multi-machine database [36]. The power fall-off length  $\lambda_q$  has been estimated as  $2/7\lambda_T$ , where  $\lambda_T$  has been evaluated at the separatrix from measurements within the database. The total sheath heat transmission factor  $\gamma$  has been fixed to 7 [45, 46]. Lastly,  $f_{
m pow}$  and  $f_{
m mom}$  have been set to 0.2 and 0, respectively, across the three devices. This choice is motivated by the fact that most of this dataset is unseeded, and, hence, momentum losses could be neglected. The obtained values for  $C_{
m 2pt}$  are 6.3, 2.2 and 2.9 in C-Mod, AUG and JET, respectively. These values are very close to those found via regression, which is a remarkable result given the large number of simplifications introduced with the two-point model.

#### 5. PREDICTIVE FORMULA AND ITS APPLICABILITY

Motivated by the overall good agreement between the regression result and the expectations from the two-point model, a fully predictive formula for  $n_{e,\text{sep}}$  is proposed, which reads:

$$n_{e,\text{sep,mod}} = C_{\text{2pt}} \cdot p_{0,\text{div}}^{0.20} \cdot I_p^{0.03} \cdot B_t^{-0.26} \cdot \left(\frac{P_{\text{SOL}}}{R_{\text{geo}}}\right)^{0.19} \cdot a_{\text{geo}}^{-0.47}, \tag{12}$$

where  $C_{\rm 2pt}$  is given by Eq. 11, and all quantities are expressed in SI units, except for  $I_p$  (MA),  $P_{\rm SOL}/R_{\rm geo}$  (MW/m) and  $n_{e,\rm sep}$  ( $10^{19}\,{\rm m}^{-3}$ ). Figure 5 shows the comparison between the predicted  $n_{e,\rm sep}$  values via Eq. 12 and the experimental values. The model is able to predict  $n_{e,\rm sep}$  within a factor 1.5 across the three tokamaks, a level of fidelity previously unmatched in the literature.

Nonetheless, many open questions on  $n_{e,\rm sep}$  prediction remain. Firstly, this database encompasses data with similar closed divertor configuration, and it is known that the divertor configuration affects the relationship between  $n_{e,\rm sep}$  and divertor parameters, such as  $T_{\rm d}$  [21, 47, 48]. Future studies should investigate whether such a complex 2D geometry dependence could be captured by simple models. Secondly, most of the database used in this study is composed of unseeded plasmas, and it is well known that (1) impurity seeding is needed in a power plant to protect the plasma facing components and (2) impurity seeding lowers  $n_{e,\rm sep}$  [49, 50, 3], as it reduces the available power to ionize neutrals in the SOL. From the two-point model perspective, impurity seeding will affect the divertor plasma temperature  $T_{\rm d}$  and, hence, the divertor neutral pressure. This change, in

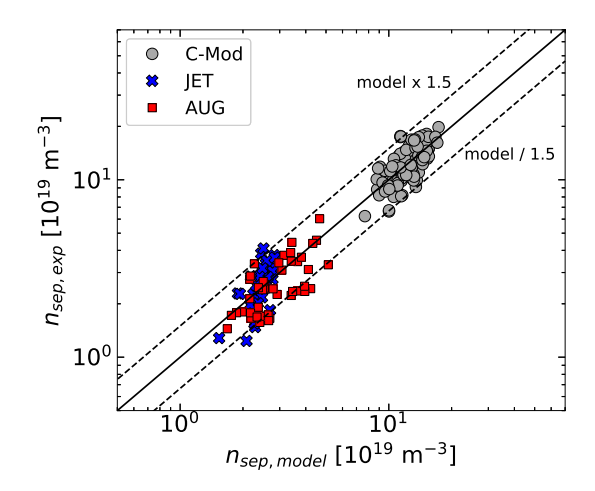


FIG. 5. Experimental  $n_{e,\rm sep}$  values against those given by the predictive formula (Eq. 12) for C-Mod (gray circles), AUG (red squares) and JET (blue triangles).

turn, will impact  $f_{\text{pow}}$  and  $f_{\text{mom}}$ , as they are a strong function of  $T_{\text{d}}$  [18, 50, 51, 52]. Future studies should investigate how this complex dynamic could be parametrized in a simple model.

#### 6. CONCLUSIONS

In this work, a multi-machine (C-Mod, AUG and JET) H-mode separatrix database is used to derive a scaling law of the separatrix electron density based on engineering parameters. Regression analysis finds  $n_{e,\rm sep}$  to scale positively with the divertor neutral pressure and  $P_{\rm SOL}/R_{\rm geo}$ , both exhibiting similar exponents ( $\sim 0.2$ ). In contrast, the parameters driving a decrease in  $n_{e,\rm sep}$  when increased are  $B_t$  and  $a_{\rm geo}$ . Interestingly,  $n_{e,\rm sep}$  is found to be independent of the plasma current, similarly to what has been observed in single machine studies upon normalization to the neutral pressure dependency [22, 25]. In this analysis, device-specific multiplication constants have been derived through regression as well, with the goal

of comparing them to the expectation from a simple model. For this purpose, the basic equations of the two-point model coupled with simple geometrical formulas have been rearranged to express  $n_{e,\rm sep}$  as a function of engineering parameters only. The obtained theoretical expression is compared to the one given by regression analysis, finding very similar device-specific multiplication constants and dependency on  $P_{\rm SOL}/R_{\rm geo}$ ,  $I_p$  and  $a_{\rm geo}$ . On the other hand, the exponents of  $p_{0,\rm div}$  and  $B_t$  are somewhat stronger and weaker in magnitude, respectively, than those found in the regression. This discrepancy could stem from additional hidden dependencies of the momentum and power loss factors on  $p_{0,\rm div}$  and  $B_t$  which cannot be captured by the model. Motivated by the overall good agreement between the regression result and the expectations from the two-point model, a fully predictive formula for  $n_{e,\rm sep}$  is proposed. This formula combines the two-point model multiplicative constant and the regression-based dependencies on  $p_{0,\rm div}$ ,  $P_{\rm SOL}/R_{\rm geo}$ ,  $I_p$ ,  $B_t$  and  $a_{\rm geo}$ . The model is able to predict  $n_{e,\rm sep}$  within a factor 1.5 across the three tokamaks, paving the way for  $n_{e,\rm sep}$  predictions in next-step devices.

#### **APPENDIX**

In this Appendix, Eq. 3 is derived. The SOL flux-tube area perpendicular to the parallel direction  $A_{\perp, SOL}$  is:

$$A_{\perp,\text{SOL}} = 2\pi R d_r \sin(\alpha) = 2\pi R d_r \frac{B_p}{B},\tag{13}$$

where R is the major radius,  $d_r$  is the radial width of the flux tube,  $\alpha$  is the magnetic field line inclination angle and  $B_p$  and B are the poloidal and total magnetic field strength, respectively. Therefore, power conservation along the flux tube from the upstream 'u' to the downstream 'd' position reads:

$$(1 - f_{\text{pow}})q_{||,\mathbf{u}}R_{\mathbf{u}}d_{r,\mathbf{u}}\frac{B_{p,\mathbf{u}}}{B_{\mathbf{u}}} = q_{||,\mathbf{d}}R_{\mathbf{d}}d_{r,\mathbf{d}}\frac{B_{p,\mathbf{d}}}{B_{\mathbf{d}}}$$

$$(1 - f_{\text{pow}})q_{||,\mathbf{u}} = q_{||,\mathbf{d}}\frac{d_{r,\mathbf{d}}}{d_{r,\mathbf{u}}}\frac{R_{\mathbf{d}}}{R_{\mathbf{u}}}\frac{B_{p,\mathbf{d}}}{B_{p,\mathbf{u}}}\frac{B_{\mathbf{u}}}{B_{\mathbf{d}}}.$$
(14)

We consider that the upstream radial width of the flux tube is the heat flux decay length at the outer midplane,  $d_{r,u} = \lambda_q$ , while the target radial width is the integral heat flux decay length multiplied by the magnetic flux expansion,  $d_{r,d} = \lambda_{int} f_{x,mag}$ . The magnetic flux expansion is defined as [53]:

$$f_{x,\text{mag}} = \frac{R_{\text{u}}}{R_{\text{d}}} \frac{B_{p,\text{u}}}{B_{p,\text{d}}}.$$
(15)

Therefore, Eq. 14 becomes:

$$(1 - f_{\text{pow}})q_{||,u} = q_{||,d} \frac{\lambda_{\text{int}}}{\lambda_q} \frac{B_{\text{u}}}{B_{\text{d}}}$$

$$(1 - f_{\text{pow}})q_{||,u} = q_{||,d} b \frac{B_{\text{u}}}{B_{\text{d}}},$$
(16)

where  $b = \lambda_{\rm int}/\lambda_q = 1 + 1.64 \cdot S$  is the divertor broadening factor. Eq. 16 can be intuitively understood by considering that the SOL cross-sectional area of the magnetic flux bundle is inversely proportional to the magnetic field strength (due to magnetic flux conservation under ideal MHD, see e.g. [54]), and that the upstream heat flux is reduced by 1/b due to the perpendicular diffusion process taking place in the divertor chamber.

#### ACKNOWLEDGEMENTS

The authors warmly acknowledge insightful discussion with O.J.W.F. Kardaun, P. Innocente, J.D. Lore, A. Pshenov and M.R.K. Wigram. This work has been carried out within the framework of the EUROfusion Consortium, funded by the European Union via the Euratom Research and Training Programme (Grant Agreement No 101052200 — EUROfusion). Views and opinions expressed are however those of the author(s) only and do not necessarily reflect those of the European Union or the European Commission. Neither the European Union nor the European Commission can be held responsible for them. This work was supported by US DOE Awards DE-SC0014264, DE-SC0021629 and was published as part of the international project co-financed by the Polish Ministry of Science and Higher Education within the programme called 'PMW' for 2023-2024.

## REFERENCES

- [1] KALLENBACH, A. et al., Nucl. Fusion 55 (2015) 053026.
- [2] EICH, T. et al., Nuclear Materials and Energy 12 (2017) 84.
- [3] DUNNE, M. G. et al., Plasma Physics and Controlled Fusion 59 (2017) 014017.
- [4] FRASSINETTI, L. et al., Nuclear Fusion **63** (2023) 112009.
- [5] HUGHES, J. et al., Nuclear Fusion 51 (2011) 083007.
- [6] OSBORNE, T. et al., Nuclear Fusion 55 (2015) 063018.

#### IAEA-CN-316/2848

- [7] SILVAGNI, D. et al., Physics of Plasmas 31 (2024) 022501.
- [8] HENDERSON, S. et al., Nuclear Materials and Energy 28 (2021) 101000.
- [9] KALLENBACH, A. et al., Plasma Physics and Controlled Fusion 58 (2016) 045013.
- [10] GOLDSTON, R. J. et al., Plasma Physics and Controlled Fusion 59 (2017) 055015.
- [11] HARRER, G. et al., Nuclear Fusion 58 (2018) 112001.
- [12] MILLER, M. et al., Nuclear Fusion 65 (2025) 052002.
- [13] SUTTROP, W. et al., Nuclear Fusion 58 (2018) 096031.
- [14] SILVAGNI, D. et al., Nuclear Fusion 63 (2023) 084001.
- [15] LIPSCHULTZ, B. et al., Nuclear Fusion 24 (1984) 977.
- [16] MAINGI, R. and MAHDAVI, M. A., Fusion Science and Technology 48 (2005) 1117.
- [17] EICH, T. et al., Nuclear Fusion 61 (2021) 086017.
- [18] STANGEBY, P. C., Plasma Physics and Controlled Fusion 60 (2018) 044022.
- [19] KRASHENINNIKOV, S. I. et al., Physics of Plasmas 23 (2016) 055602.
- [20] LEONARD, A. et al., Nuclear Fusion 57 (2017) 086033.
- [21] LOMANOWSKI, B. et al., Nuclear Fusion 63 (2023) 036019.
- [22] KALLENBACH, A. et al., Plasma Physics and Controlled Fusion 60 (2018) 045006.
- [23] KALLENBACH, A. et al., Nuclear Materials and Energy 18 (2019) 166.
- [24] STAGNI, A. et al., Nuclear Fusion 64 (2024) 026016.
- [25] SILVAGNI, D. et al., Nuclear Materials and Energy 42 (2025) 101867.
- [26] LUDA, T. et al., Nuclear Fusion 60 (2020) 036023.
- [27] GREENWALD, M. et al., Physics of Plasmas 6 (1999) 1943.
- [28] TOLMAN, E. et al., Nuclear Fusion 58 (2018) 046004.
- [29] GIROUD, C. et al., Plasma Physics and Controlled Fusion 57 (2015) 035004.
- [30] GIROUD, C. et al., Nuclear Fusion 64 (2024) 106062.
- [31] PSHENOV, A. et al., Nuclear Materials and Energy 42 (2025) 101851.
- [32] ERENTS, S. et al., Nuclear Fusion 40 (2000) 309.
- [33] FRASSINETTI, L. et al., Nuclear Fusion 65 (2025) 076028.
- [34] HARRISON, J. R. et al., Plasma Physics and Controlled Fusion (2024).
- [35] EICH, T. et al., Phys. Rev. Lett. 107 (2011) 215001.
- [36] EICH, T. et al., Nuclear Fusion 53 (2013) 093031.
- [37] MAKOWSKI, M. A. et al., Phys. Plasmas 19 (2012) 056122.
- [38] LUNT, T. et al., Nuclear Materials and Energy 12 (2017) 1037.
- [39] LUNT, T. et al., Phys. Rev. Lett. 130 (2023) 145102.
- [40] UCKAN, N. A. and ITER Physics Group, *ITER physics design guidelines: 1989*, International Atomic Energy Agency (IAEA), 1990.
- [41] OSBORNE, N. et al., Nuclear Fusion, accepted (2025).
- [42] TERRY, J. et al., Journal of Nuclear Materials 438 (2013) S212.
- [43] BRUNNER, D. et al., Nuclear Fusion 58 (2018) 076010.
- [44] PITTS, R. et al., Journal of Nuclear Materials 337-339 (2005) 146.
- [45] STANGEBY, P., The Plasma Boundary of Magnetic Fusion Devices, Bristol: Institute of Physics Publishing, 2000.
- [46] BRIDA, D. et al., Plasma Physics and Controlled Fusion 62 (2020) 105014.
- [47] GROTH, M. et al., Journal of Nuclear Materials 463 (2015) 471.
- [48] MOULTON, D. et al., Pumping in vertical and horizontal target configurations on JET in L-mode; an interpretive study using EDGE2D-EIRENE, in 42nd EPS Conf. on Plasma Physics, Lisbon, Portugal, O4.119, 2015.
- [49] PACHER, H. et al., Journal of Nuclear Materials 463 (2015) 591.
- [50] LORE, J. et al., Nuclear Fusion 62 (2022) 106017.
- [51] LIPSCHULTZ, B. et al., Fusion Science and Technology 51 (2007) 369.
- [52] Paradela Pérez, I. et al., Nuclear Materials and Energy 12 (2017) 181.
- [53] LOARTE, A. et al., Journal of Nuclear Materials 266-269 (1999) 587.
- [54] ZOHM, H., Magnetohydrodynamic Stability of Tokamaks, WILEY-VCH, 2015.